

Strictly Non-Blocking Silicon Photonics Switches

Keijiro SUZUKI^{†a)}, Ryotaro KONOIKE[†], Members, Satoshi SUDA[†], Nonmember, Hiroyuki MATSUURA[†], Shu NAMIKI[†], Hitoshi KAWASHIMA[†], and Kazuhiro IKEDA[†], Members

SUMMARY We review our research progress of multi-port optical switches based on the silicon photonics platform. Up to now, the maximum port-count is 32 input ports \times 32 output ports, in which transmissions of all paths were demonstrated. The switch topology is path-independent insertion-loss (PILOSS) which consists of an array of 2 \times 2 element switches and intersections. The switch presented an average fiber-to-fiber insertion loss of 10.8 dB. Moreover, -20 -dB crosstalk bandwidth of 14.2 nm was achieved with output-port-exchanged element switches, and an average polarization-dependent loss (PDL) of 3.2 dB was achieved with a non-duplicated polarization-diversity structure enabled by SiN overpass waveguides. In the 8 \times 8 switch, we demonstrated wider than 100-nm bandwidth for less than -30 -dB crosstalk with double Mach-Zehnder element switches, and less than 0.5 dB PDL with polarization diversity scheme which consisted of two switch matrices and fiber-type polarization beam splitters. Based on the switch performances described above, we discuss further improvement of switching performances.

key words: silicon photonics, optical switches, photonic integrated circuits, optoelectronics

1. Introduction

Demand for cloud-services generates massive data flows in data centers [1]. To handle the data flow, fast and energy-efficient network systems based on optical switches attract attention [2], [3]. Figure 1 summarizes several kinds of optical switches, in which their port counts are plotted against the switching time. Free-space optical switches (Piezo actuator and MEMS mirror) can provide hundreds of switching ports. However, their switching time is longer than 1 ms. Generally speaking, the switches for the data centers are required less than 1 ms switching time [2], and hence the silica switches are also challenging to deploy them. On the other hand, integrated switches based on semiconductors (Si, InP, etc.) can provide from several tens of μ s to 1 ns switching time. As for the port count, some reports say that a port count of 32 is acceptable for the large scale data centers [2], and which is achievable port count for the integrated switches.

Among several kinds of the integrated switch platforms and switching architectures, we focused on the Si photonics with thermo-optic phase shifter. The Si photonics platform possesses high-density and homogeneous integration and

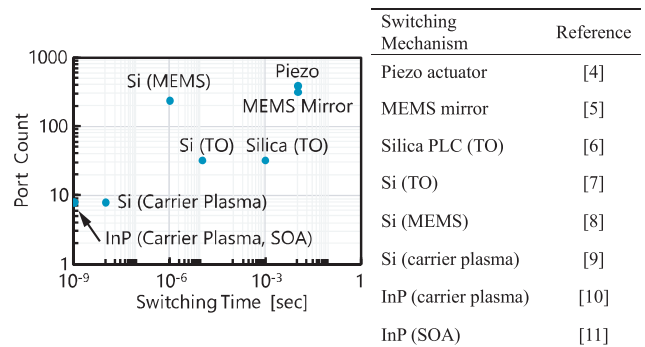


Fig. 1 Summary of optical switch technologies. MEMS: micro electro mechanical systems, TO: thermo-optic. SOA: semiconductor optical amplifier

mass-producibility enabling low-cost production. Moreover, the thermo-optic phase shift offers low-loss switching with the order of a microsecond. Therefore, we think that the combination is suitable for the multi-port optical switch.

As for the Si photonics with carrier plasma phase-shift, it can operate nanoseconds order. However, the loss caused by the carriers is a problem for the optical switches in which element switches are cascaded. Similarly, the InP platform with carrier plasma has the same challenge. Although the SOA based switch can provide nanoseconds order switching with low-loss, the large scale integration is difficult due to fabrication and energy concerns. The Si photonics with the MEMS switch enables large port count (more than 200) and less than microseconds switching with low insertion loss. However, its electrical packaging is challenging, and hence transmissions of all-paths have not been demonstrated yet.

In this paper, we review our researches and developments of Si-photonics strictly non-blocking multi-port switches. This paper is composed as follows. In Sect. 2, we discuss the reduction of the fiber-to-fiber insertion loss, and 32 input port \times 32 output port optical switch. In Sect. 3, we describe operating bandwidth expansion. In Sect. 4, we describe polarization-independent operation. In Sect. 5, we discuss further improvement of the switching performances. Finally, in Sect. 6, we conclude this paper.

2. Fiber-to-Fiber Insertion Loss

The fiber-to-fiber insertion loss of the multi-port switch includes propagation loss of the Si waveguides, the insertion loss of the intersections, and fiber-to-chip coupling losses.

Manuscript received December 16, 2019.

Manuscript revised March 13, 2020.

Manuscript publicized April 17, 2020.

[†]The authors are with National Institute of Advanced Industrial Science and Technology (AIST), Tsukuba-shi, 305–8596 Japan.

a) E-mail: k.suzuki@aist.go.jp

DOI: 10.1587/transele.2019OCP0001

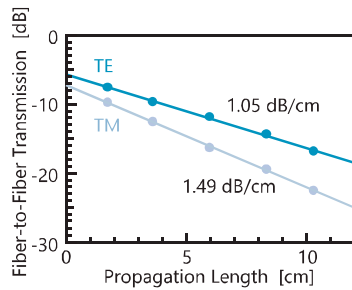


Fig. 2 Propagation loss of Si waveguide fabricated on semiconductor-on-insulator wafer by using immersion ArF lithography at a wavelength of $1.55 \mu\text{m}$.

Here, we assumed that the insertion loss of the element Mach-Zehnder (MZ) switch is included in the propagation loss of the Si waveguide because the element MZ switch consists of the thermo-optic phase shifters and directional couplers (DCs), which are inherently lossless components.

Figure 2 shows the propagation loss of the Si waveguide, which is 430-nm wide and 220-nm thick. The measured propagation losses of the transverse electric (TE) like mode and that of the transverse magnetic (TM) like mode were 1.05 dB/cm and 1.49 dB/cm, respectively. The Si waveguide is defined with an immersion ArF lithography to reduce the sidewall roughness and variation of waveguide core width. Compared with a KrF lithography, in general, higher resolution and homogeneity of the immersion ArF lithography provide higher optical performances and yield. The propagation loss for the TE-like mode is lower than that of the TM-like mode, indicating that the main contribution to the propagation loss is not side-wall roughness.

The intersections are important components for the multi-port optical switches because the multi-port switch contains many intersections. Their insertion loss and leakage to an opposite output port (i.e. crosstalk) affect the optical performances of the whole switch matrix. As the intersections, we use an adiabatic taper intersection which is numerically optimized [12]. Figure 3 (a) presents the transmission spectra of the fabricated test device. The through-port transmission spectrum exhibits flat response against wavelength. The leakage spectrum is lower than that of the through-port by $< -47 \text{ dB}$. The insertion loss of the intersection is 0.024 dB, as shown in Fig. 3 (b). This insertion loss is acceptable for the multi-port switch which has several tens of input/output ports. For example, 32×32 switch has 31 intersections on a path, contributing $0.024 \text{ dB} \times 31 = 0.74 \text{ dB}$ loss.

The fiber-to-chip coupling loss is one of the largest causes of the insertion loss due to the mode field profile mismatch between the optical fiber and the Si waveguide. To minimize the coupling loss, we developed an optical connector based on a high- Δ optical fiber array and an extremely high- Δ silica planar lightwave circuit (PLC) [13]. A standard single-mode fiber (SMF) is connected to the high- Δ fiber by a thermally-diffused expanded core technique. The high- Δ optical fiber is butt-coupled to the PLC, in which the fiber pitch is $127 \mu\text{m}$. In the PLC, the fiber pitch is reduced

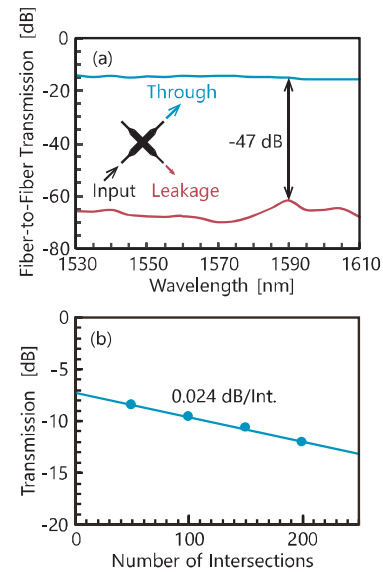


Fig. 3 (a) Through-port transmission and leakage spectra of adiabatic taper intersection. (b) Insertion loss at a wavelength of $1.55 \mu\text{m}$. The intersection is designed for the TE-like mode.

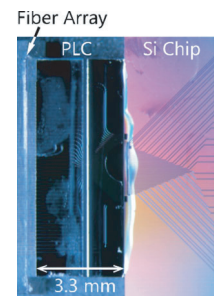


Fig. 4 Microscope image of connection facet between extremely-high- Δ PLC connector and Si chip.

to $50 \mu\text{m}$. Finally, the PLC is butt-coupled to the Si chip with a UV-cured glue, as shown in Fig. 4. The structure of the edge coupler on the chip is conventional inverse-taper, of which core width is 170 nm for the TE mode and 140 nm for the TM mode. For the TE mode, we demonstrated an average SMF to Si-waveguide loss of 1.54 dB/facet (Max: 1.6 dB/facet, Min: 1.4 dB/facet), and negligible wavelength dependence over C and L band.

By using the technologies and the components described above, we fabricated a 32×32 path-independent insertion loss (PILOSS) switch. The PILOSS topology gives strictly non-blocking switch with the lowest on-chip loss [14]. The switch chip was prepared with a CMOS pilot line. The two facets of the chip having the edge couplers were polished, then the electrodes on the chip were flip-chip bonded to a ceramic interposer. After that, the optical connectors were attached to the polished edge. Finally, the interposer was inserted into a socket on a printed circuit board with control electronics. Figure 5 shows the assembled 32×32 switch. The 32×32 switch was composed of 1024 element MZ switches, and which were controlled with a pulse width modulation technique [15].

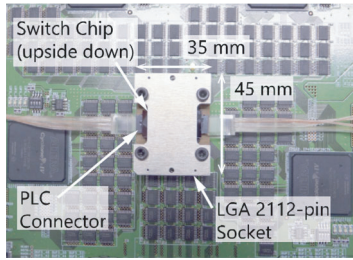


Fig. 5 Fabricated 32×32 switch assembled on control board.

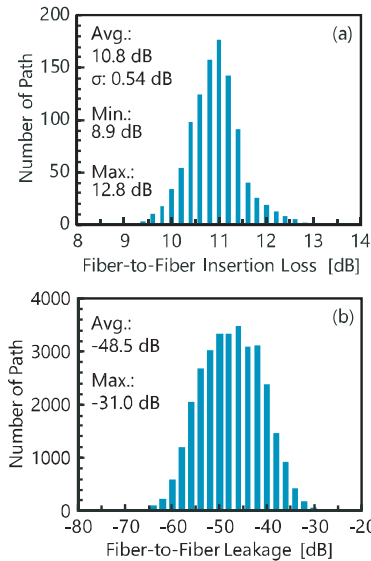


Fig. 6 (a) Fiber-to-fiber insertion loss and (b) leakages to non-target port distributions of 32×32 switch at a wavelength of $1.547 \mu\text{m}$.

Figure 6(a) shows the distribution of the measured fiber-to-fiber insertion losses of all 1024 paths. The maximum, minimum, and average insertion losses were 12.8 dB, 8.9 dB, and 10.8 dB, respectively. The standard deviation was 0.54 dB. The minimum insertion loss includes the following losses: 1.4 dB SMF-to-chip coupling loss, 0.70 dB propagation loss of an input routing waveguide, 4.0 dB insertion loss of the MZ switches, 0.74 dB insertion loss of the intersections, 0.63 dB propagation loss of an output routing waveguide, and 1.4 dB chip-to-SMF coupling loss. Figure 6(b) shows the distribution of the leakages which are output powers from non-target output ports. The maximum, and average leakages were -31.0 dB, and -48.5 dB, respectively.

3. Operating Bandwidth Expansion

In the DC-based MZ switch shown in Fig. 7(a), the low-crosstalk bandwidth is limited by the wavelength dependence of the DC. A straightforward way to achieve broadband operation is replacing the DCs to some broadband couplers such as multi-mode interference (MMI) couplers or adiabatic DCs. However, the MMI possesses high (~ 0.5 dB) insertion loss, and the adiabatic DCs requires se-

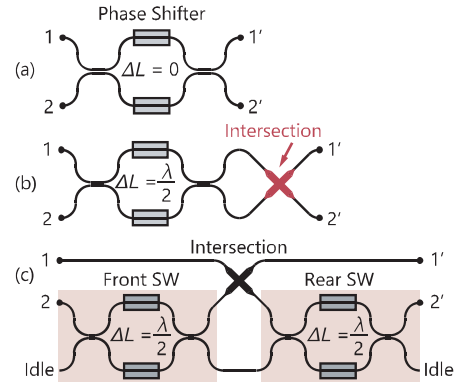


Fig. 7 (a) Conventional Mach-Zehnder (MZ) switch based on directional coupler. (b) Output-port-exchanged MZ switch. (c) Double-MZ switch.

vere (< 0.1 nm) fabrication control. Therefore, we decided to evaluate two kinds of the element switches: an output-port exchanged MZ switch (Fig. 7(b)) [16], and a double-MZ switch (Fig. 7(c)) [17]. These are originally proposed in the silica PLC platform.

In PILOSS switch, most of the element switches are in the cross-state (input port 1 (2) is connected to output port 2' (1')), and the leakage to the bar-port (output port 1' (2')) when the input port is 1 (2)) becomes the crosstalk. Therefore, the suppression of the leakages to the bar-port is important. However, according to the coupled-mode theory, the complete suppression of the leakage to the bar-port occurs only for a wavelength in which the splitting ratio of the two 3-dB couplers is exactly 50 : 50 or complementary [18]. This indicates that bar-port suppression possesses high wavelength dependence. On the other hand, the complete leakage suppression to the cross-port (output port 2' (1')) when the input port is 1 (2)) requires identical splitting ratios even though they are not equal to 50 : 50. This means that the cross-port suppression exhibits low wavelength dependence. Based on these facts, the output-port exchanged MZ switch can expand the low crosstalk bandwidth [19].

The double-MZ switch provides broad low crosstalk bandwidth because the leakage from the front MZ switch is suppressed with the rear MZ switch. In the cross-state, input port 1 (2) is connected to output-port 2' (1'). In the bar-state, input-port 2 is connected to output-port-2'. The connection from input-port 1 to output-port 1' is not necessary for PLOSS topology in which the element double-MZ switches are placed normal and upside-down positions in turns [20]. In this PILOSS switch, the number of the MZ switches on a path increases by one, and that of the intersections increases by $N - 1$ for $N \times N$ switch.

Figure 8 compares the measured fiber-to-fiber transmission spectra of one of the severest paths and the sum of leakages to the severest path among the three element-MZ-switches. Here, the crosstalk is defined as a ratio between the insertion loss of the path and the sum of leakages from other paths. In the standard MZ switch shown in Fig. 8(a), -20 -dB crosstalk bandwidth was 3.5 nm [7]. By using the output-port exchanged MZ switch, -20 dB crosstalk

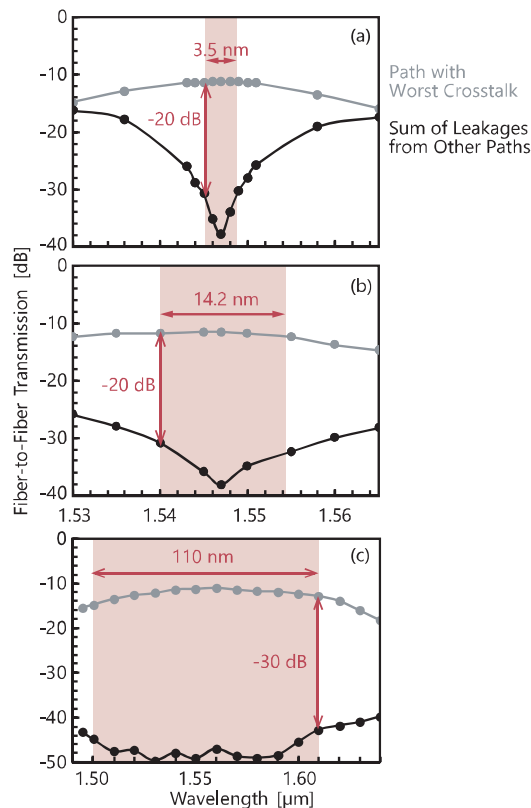


Fig. 8 Measured fiber-to-fiber transmission spectra of one of the severest paths and sum of leakages from other paths. (a) 32×32 switch based on conventional Mach-Zehnder (MZ) element switches. (b) 32×32 switch based on output-port-exchanged MZ element switches. (c) 8×8 switch based on double-MZ element switches.

bandwidth was expanded to 14.2 nm (Fig. 8(b)), corresponding to four times expansion [19]. Figure 8(c) presents the crosstalk of the double-MZ 8×8 PILOSS switch. Although the port count is 8×8 , -30 dB crosstalk bandwidth covers 110 nm wavelength range [21]. As shown in Fig. 8, the low crosstalk bandwidth is expanded by using the modified element switches. However, there is some drawbacks: an increase in the number of intersections, the MZ switches, etc. The pros and cons will be discussed in Sect. 5.

4. Polarization Independent Operation

Polarization-independent operation is another important characteristic because the optical switches deal with dual-polarization, and/or polarization scrambled signals. To achieve this, we chose a polarization-diversity scheme. Although the polarization-insensitive devices are alternative options, we think that they are not realistic options in the silicon photonics platform because they require thick ($\sim 1.5 \mu\text{m}$) silicon waveguide core [22], or precise fabrication control beyond the capability of typical CMOS-based pilot line [23].

As the polarization-diversity schemes, we exploited three schemes: off-chip (Fig. 9(a)) [20], on-chip (Fig. 9(b)) [14], and non-duplicated polarization diversity

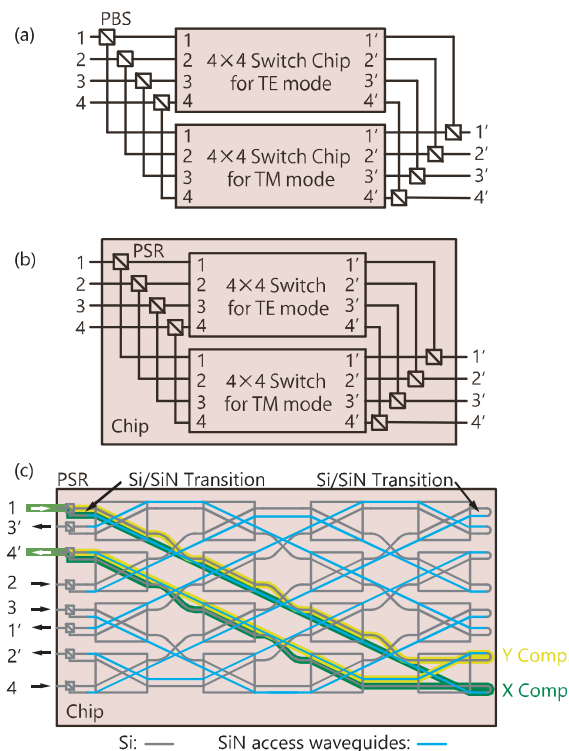


Fig. 9 Polarization-diversity schemes (a) based on polarization beam splitter with fiber pig-tails, (b) based on polarization splitter rotators integrated on chip, and (c) based on non-duplicated switch matrix configuration with SiN overpass access waveguides.

schemes (Fig. 9(c)) [24]. The off-chip scheme consists of the two switch chips, which are packaged on each control board, and polarization beam splitters (PBSs) with fiber pig-tails. The originally TE mode (X component) propagates the switch chip through the input PBS, then is converted to the TM mode with the output PBS. The originally TM mode (Y component) is separated with the input PBS, then is launched to another switch chip as the TE mode. The output from the switch chip is combined with the X component. Hence, X and Y components are exchanged. The on-chip diversity scheme works as the same fashion as the off-chip diversity except that the PBSs are replaced with on-chip polarization splitter rotators (PSRs) and all the components are integrated into a single switch chip. The non-duplicated diversity scheme utilizes full ports of PILOSS topology and SiN overpass waveguides. X component is separated by using the input PSR and is transferred to the SiN overpass waveguide layer. After the propagation to the right side of the switch matrix, the X component is transferred to the Si waveguide layer. X component propagates switch matrix from right to left, then is converted into the TM mode and combined with Y component in the output PSR. Y component is separated and converted to TE mode with the input PSR, then propagates the switch matrix from left to right. After the transfer to the SiN overpass waveguide layer, the Y component comes back to the left side, then is transferred to the Si waveguide layer. Finally, the Y component is combined with the X component with the output PSR.

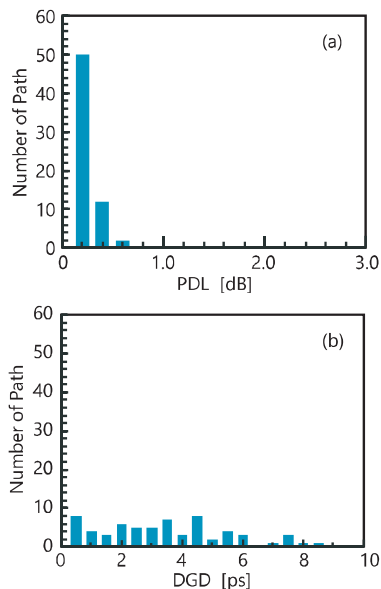


Fig. 10 Distributions of (a) polarization-dependent and (b) differential group delay of polarization-diversity 8×8 switch based on polarization-beam splitters with fiber pigtail. The wavelength was set to $1.535 \mu\text{m}$.

We composed an off-chip polarization-diversity 8×8 switch [20]. Figure 10(a) shows the distribution of the polarization-dependent loss (PDL) of all (64) paths at a wavelength of $1.535 \mu\text{m}$. The PDL was less than 0.5 dB. We infer that the residual PDL is caused by the polarization fluctuation of the experimental setup. Figure 10(b) shows the distribution of the differential group delay (DGD) of all paths. The DGD was less than 8.5 ps. This DGD is attributed to optical fiber length (from the PBS to the Si chip) difference ($< 1 \text{ mm}$) between the two polarizations. These results indicate that the off-chip diversity can achieve low PDL, however, approximately 10 ps DGD is inevitable.

Next, we fabricated the on-chip diversity 8×8 switch [14]. In the on-chip diversity switch, we used the on-chip PSR based on mode conversion and vertically-asymmetric directional-coupling using a rib waveguide [25]. Figure 11(a) shows the structure of the PSR. The TE mode propagates through the PSR to output 2'. The TM mode is converted to the first order TE mode with tapered waveguide, then coupled to the fundamental TE mode of the adjacent waveguide. The fundamental TE mode propagates to output port 1'. Figure 11(b) presents the transmission spectra in the case of the TE mode input. Most of the input TE mode propagates to output port 2' (TE2'). TM2' indicates that the residual TM component of the input light, and which can be eliminated if a polarization cleaner was placed on the output of the PSR. Figure 11(c) shows the transmission spectra in the case of the TM mode input. The TM mode propagates to output port 1' (TE1'). The component of TM2' can be also eliminated with the polarization cleaner. The insertion loss was estimated to be less than 4-dB in the C and L band. This insertion loss contains the insertion loss of the PSR itself and the loss related to the residual TM component which is suppressed with a

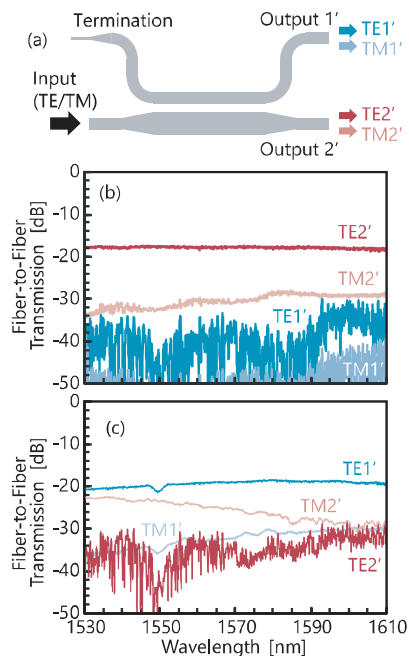


Fig. 11 (a) Schematic of polarization-splitter-rotator. (b) Transmission spectra of each output port in case of TE-like mode input. (c) TM-like mode.

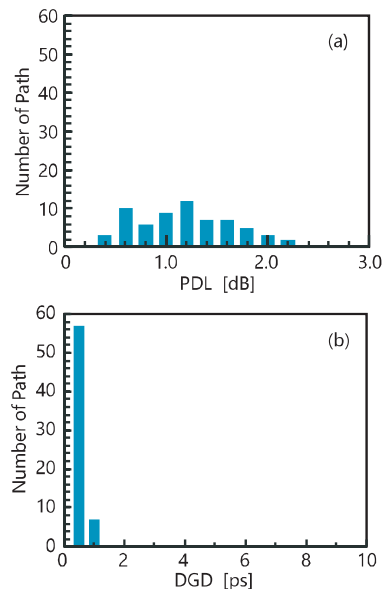


Fig. 12 Distributions of (a) polarization-dependent loss and (b) differential group delay of polarization-diversity 8×8 switch based on polarization splitter rotators integrated on chip. The wavelength was set to $1.550 \mu\text{m}$.

successive polarization cleaner.

Figure 12 shows the PDL of the on-chip diversity 8×8 switch. The PDL was less than 2.1 dB. We infer that this PDL is caused by the variation of the insertion loss of the PSR. If we made a new design for the PSR to be robust to the structural variation, the PDL would be improved. On the other hand, the DGD shown in Fig. 12(b) is less than 1-ps owing to full integration and path length equalized design.

Finally, we describe the optical characteristics of a

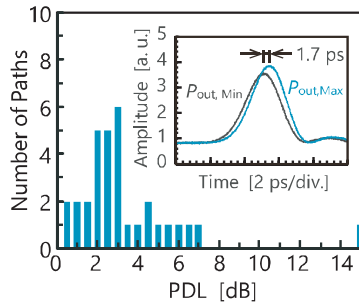


Fig. 13 Distribution of polarization-dependent loss of at a wavelength of $.1547 \mu\text{m}$. 32 paths were sampled from 1024 paths of the non-duplicated polarization-diversity 32×32 switch. The sampled paths are 1 (input) – 1' (output), 2 – 2', 3 – 3', ..., 32 – 32'.

non-duplicated diversity 32×32 switch [24]. Figure 13 shows the distribution of the PDL, in which 32 paths (1 (input) – 1' (output), 2 – 2', 3 – 3', ..., 32 – 32') were sampled. The average PDL was 3.5 dB and the minimum one was 0.32 dB. Moreover, 75% of paths exhibited less than 3 dB PDL. We guess that there are two reasons for the PDL. The one is the interference between the light propagating the composed path and the leakages from the path composed for the opposite polarization component. The other is insufficient polarization splitting and rotating at the PSRs. Therefore, there are some rooms for the improvement of the optical characteristics by optimizing the device design, fiber-to-chip coupling, and the calibration procedures of the element switches. The inset of Fig. 13 shows optical pulses that propagated the switch. By comparing the delay of the two pulses, in which the polarizations were controlled the maximum and minimum output power, the DGD was estimated to be 1.7 ps.

5. Outlook

In this section, we describe our outlook for the performances of the Si optical switches, including fiber-to-fiber insertion loss, broadband and polarization-insensitive operations, and port-count expansion.

As for the fiber-to-fiber insertion loss, we guess that approximately 6-dB in the 32×32 switch is achievable by adopting the optimized fabrication process (propagation loss: 0.5 dB/cm) and the edge coupling (coupling loss (numerical simulation): 0.6 dB/facet). Regarding the broadband operation, we believe that the double-MZ switch is one of the most suitable options. By adopting the double-MZ switch, the number of the MZ switch and the intersection on a path for $N \times N$ switch become $N + 1$ and $2(N - 1)$, respectively. This means that the additional one MZ switch and $(N - 1)$ intersections are inserted into a path by comparing conventional MZ-switch based PILOSS switch. We think that these increments are acceptable because the loss increment from additional components is acceptable. For example, in 32×32 switch, the loss increment would be 0.13 dB from the MZ switch and $0.024 \text{ dB} \times 31 = 0.74 \text{ dB}$ from the intersections. For polarization-insensitivity, we

think that a polarization-diversity scheme is a realistic option as described in Sect. 4.

The port-count expansion is a remaining challenge. The port-count is limited by electrical packaging. In our 32×32 switch, 2112 electrodes were drawn out to the control board with the land grid array. If we compose a 64×64 switch by simply expanding the PILOSS topology, we would have 8320 electrodes. Hence, we have to develop some new technology to reduce the number of electrodes, for example, the dynamic control of the phase-shifters [26], the integration with an address decoder, etc.

6. Conclusion

We have reviewed our silicon-photonics strictly non-blocking optical switches. The 32×32 switch is the largest port count switch which exhibits the full port operation. The switch was electrically and optically packaged. We demonstrated an average fiber-to-fiber insertion loss of 10.8 dB. We guess that the 6 dB insertion loss, which is comparable to that of the silica switch, is achievable by the improvement of our fabrication and packaging processes. The double-MZ 8×8 switch exhibited 110 nm bandwidth for less than -30 dB crosstalk. Furthermore, the polarization-insensitive operation was demonstrated with the polarization-diversity scheme. As a remaining challenge, we noticed that port count expansion which requires some new packaging and/or controls technology for the reduction of the number of electrodes. Moreover, loss reduction and simultaneous achievement of the low PDL and the low DGD should be addressed. Although there are some remaining challenges, we think that the silicon photonics multi-port switches can bring new functionality to networks for the data centers and telecom systems.

Acknowledgments

This work is partly conducted through TIA-VICTORIES Open Innovation Hub.

References

- [1] Cisco Global Cloud Index: Forecast and Methodology, 2016–2021 White Paper.
- [2] Q. Cheng, S. Rumley, M. Bahadori, and K. Bergman, "Photonic switching in high performance datacenters [invited]," *Opt. Express*, vol.26, no.12, pp.16022–16043, 2018/06/11, 2018.
- [3] B.G. Lee and N. Dupuis, "Silicon photonic switch fabrics: Technology and architecture," *J. Lightwave Technol.*, vol.37, no.1, pp.6–20, 2019.
- [4] Polatis, web page: <https://www.polatis.com/>
- [5] Calient, web page, <https://www.calient.net/>
- [6] S. Sohma, T. Watanabe, N. Ooba, M. Itoh, T. Shibata, and H. Takahashi, "Silica-based plc type 32×32 optical matrix switch," *European Conference on Optical Communications (ECOC)*, p.Tu.4.4.3, IEEE, Cannes, France, 2006.
- [7] K. Suzuki, R. Konoike, J. Hasegawa, S. Suda, H. Matsuura, K. Ikeda, S. Namiki, and H. Kawashima, "Low-insertion-loss and power-efficient 32×32 silicon photonics switch with extremely high- δ silica plc connector," *J. Lightwave Technol.*, vol.37, no.1,

- pp.116–122, 2019.
- [8] T.J. Seok, K. Kwon, J. Henriksson, J. Luo, and M.C. Wu, “Wafer-scale silicon photonic switches beyond die size limit,” *Optica*, vol.6, no.4, pp.490–494, 2019/04/20, 2019.
- [9] L. Qiao, W. Tang, and T. Chu, “ 32×32 silicon electro-optic switch with built-in monitors and balanced-status units,” *Sci Rep-Uk*, vol.7, p.42306, 02/09/online, 2017.
- [10] M.-J. Kwack, T. Tanemura, A. Higo, and Y. Nakano, “Monolithic inp strictly non-blocking 8×8 switch for high-speed wdm optical interconnection,” *Opt. Express*, vol.20, no.27, pp.28734–28741, 2012/12/17, 2012.
- [11] Q. Cheng, A. Wonfor, J.L. Wei, R.V. Penty, and I.H. White, “Low-energy, high-performance lossless 8×8 soa switch,” *Optical Fiber Communication Conference*, p.Th4E.6, Optical Society of America, Los Angeles, California, 2015.
- [12] Y. Ma, Y. Zhang, S. Yang, A. Novack, R. Ding, A.E. Lim, G.-Q. Lo, T. Baehr-Jones, and M. Hochberg, “Ultralow loss single layer submicron silicon waveguide crossing for soi optical interconnect,” *Opt Express*, vol.21, no.24, pp.29374–29382, Dec. 02, 2013.
- [13] J. Hasegawa, K. Ikeda, K. Suzuki, S. Yamasaki, G. Kobayashi, M. Takahashi, and H. Kawashima, “ 32 -port 5.5% - δ silica-based connecting device for low-loss coupling between smfs and silicon waveguides,” *Optical Fiber Communication Conference*, p.Tu3A.4, Optical Society of America, San Diego, California, 2018.
- [14] K. Suzuki, R. Konoike, S. Suda, H. Matsuura, S. Namiki, H. Kawashima, and K. Ikeda, “Low-loss, low-crosstalk, and large-scale optical switch based on silicon photonics,” *J. Lightwave Technol.*, 2019, DOI: 10.1109/JLT.2019.2934768 (early access).
- [15] K. Tanizawa, K. Suzuki, S. Suda, H. Matsuura, K. Ikeda, S. Namiki, and H. Kawashima, “Silicon photonic 32×32 strictly-non-blocking blade switch and its full path characterization,” 2016 21st Optoelectronics and Communications Conference (OECC) Held Jointly With 2016 International Conference on Photonics in Switching (Ps), p.PD2-3, IEICE, Niigata, Japan, 2016.
- [16] M. Okuno, K. Kato, R. Nagase, A. Himeno, Y. Ohmori, and M. Kawachi, “Silica-based 8×8 optical matrix switch integrating new switching units with large fabrication tolerance,” *J. Lightwave Technol.*, vol.17, no.5, pp.771–781, 1999/05/01, 1999.
- [17] T. Goh, A. Himeno, M. Okuno, H. Takahashi, and K. Hattori, “High-extinction ratio and low-loss silica-based 8×8 strictly nonblocking thermo-optic matrix switch,” *J. Lightwave Technol.*, vol.17, no.7, pp.1192–1199, 1999.
- [18] K. Suzuki, G. Cong, K. Tanizawa, S.-H. Kim, K. Ikeda, S. Namiki, and H. Kawashima, “Ultra-high-extinction-ratio 2×2 silicon optical switch with variable splitter,” *Opt. Express*, vol.23, no.7, pp.9086–9092, 2015/04/06, 2015.
- [19] K. Suzuki, R. Konoike, S. Suda, H. Matsuura, S. Namiki, H. Kawashima, and K. Ikeda, “Low-crosstalk bandwidth expansion in 32×32 silicon optical switch with port-exchanged mach-zehnder switch,” *OptoElectronics and Communications Conference (OECC) / International Conference on Photonics in Switching and Computing (PSC)*, p.J1-3, IEICE, Fukuoka, 2019.
- [20] K. Suzuki, K. Tanizawa, S. Suda, H. Matsuura, T. Inoue, K. Ikeda, S. Namiki, and H. Kawashima, “Broadband silicon photonics 8×8 switch based on double-mach-zehnder element switches,” *Opt. Express*, vol.25, no.7, pp.7538–7546, April 2017, 2017.
- [21] K. Suzuki, K. Tanizawa, S. Suda, H. Matsuura, K. Ikeda, S. Namiki, and H. Kawashima, “ 2.5 -db loss, 100 -nm operating bandwidth, and low power consumption strictly-non-blocking 8×8 si switch,” *European Conference on Optical Communication (ECOC)*, p.Tu.1.C.2, Gothenburg, 2017.
- [22] S. Nakamura, S. Yanagimachi, H. Takeshita, A. Tajima, T. Hino, and K. Fukuchi, “Optical switches based on silicon photonics for roadm application,” *IEEE J. Sel. Topics Quantum Electron.*, vol.22, no.6, p.3600609, 2016.
- [23] S. Han, T.J. Seok, K. Yu, N. Quack, R.S. Muller, and M.C. Wu, “ 50×50 polarization-insensitive silicon photonic mems switches: Design and experiment,” *European Conference and Exhibition on Optical Communications (ECOC)*, p.Th.3.A.5, Düsseldorf, 2016.
- [24] oK. Suzuki, R. Konoike, N. Yokoyama, M. Seki, M. Ohtsuka, S. Saitoh, S. Suda, H. Matsuura, K. Yamada, S. Namiki, H. Kawashima, and K. Ikeda, “Nonduplicate polarization-diversity 32×32 silicon photonics switch based on a sin/si double-layer platform,” *J. Lightwave Technol.*, 2019, DOI: 10.1109/JLT.2019.2934763 (early access).
- [25] D. Dai and J.E. Bowers, “Novel concept for ultracompact polarization splitter-rotator based on silicon nanowires,” *Opt. Express*, vol.19, no.11, pp.10940–10949, 2011/05/23, 2011.
- [26] A. Ribeiro and W. Bogaerts, “Thermo-optical phase shifter with integrated diodes for multiplexed control,” *Optical Fiber Communication Conference*, p.Th2A.4, Optical Society of America, San Diego, California, 2018.



Keijiro Suzuki received his BE and ME degrees from the Department of Electrical and Electronic Engineering, Shizuoka University, Hamamatsu, Japan, in 2004 and 2006, respectively. After spending two years at Sumitomo Osaka Cement Co., Ltd., he entered the Department of Electrical and Computer Engineering, Yokohama National University (YNU), Yokohama, Japan, in 2008 and was awarded the Research Fellowship for Young Scientists from JSPS. He received his Ph.D. degree from YNU in 2011. After spending one year at YNU as a post-doctoral fellow, he joined National Institute of Advanced Industrial Science and Technology (AIST), Tsukuba, Japan, in 2012. He is a member of the OSA, the IEICE, and the JSAP. His research interests include photonic integrated circuits, nanophotonics, and nonlinear optics.



Ryotaro Konoike received his MS and PhD degrees from the Department of Electronic Science and Engineering, Kyoto University, Japan, in 2014 and 2017, respectively. At Kyoto University, he studied the integration of manipulation of photons on a photonic crystal chip containing multiple coupled nanocavities. He is currently a researcher with the National Institute of Advanced Industrial Science and Technology (AIST), Japan. His research interests include optical switches and integrated silicon photonic circuits.



Satoshi Suda was born in Kobe, Japan, in 1979. He received his BS, MS, and PhD degrees in science and engineering from Tokyo Institute of Technology, Yokohama, Japan, in 2003, 2004, and 2008, respectively. His Ph.D. work was on optical nonlinear devices based on a vertical cavity surface emitting laser in telecommunication wavelength. He joined the National Institute of Advanced Industrial Science and Technology, Tsukuba, Japan, in 2008, where he has been engaged in the research on silicon photonics circuits.



Hiroyuki Matsuura received his BS and MS degrees in Electrical engineering from Tokyo Institute of Technology, Tokyo, Japan, in 1978 and 1980, respectively. In 1980, he joined Yokogawa Electric Corporation, Tokyo, Japan, where he was engaged in the research on medical imaging apparatuses, high-frequency circuits, and measuring instruments. From 1990 to 1992, he was a visiting scholar at Stanford University, Stanford, CA. From 1992 to 2011, he was engaged in the technology development

of high-speed, high-frequency circuits with compound semiconductors and business development for optical communication modules in Yokogawa Electric Corporation. Since 2011, he has been a senior researcher in the National Institute of Advanced Industrial Science and Technology, Tsukuba, Japan and involved in the development of control circuits and units for next-generation optical communication devices and systems. In 2017, he established HikariPath Communications Co., Ltd., which provides low-latency, high-resolution, and bi-directional video transmission services using optical technologies. Mr. Matsuura is a member of the Institute of Electrical and Electronics Engineers (IEEE) and the Institute of Electronics, Information and Communication Engineers (ICICE). He was a recipient of the 1988 Society of Instrument Control Engineers (SICE) Best Paper Award.



Shu Namiki received M.S. and Dr. Sci. degrees in applied physics from Waseda University, Tokyo, Japan, in 1988 and 1998, respectively. From 1988 to 2005, he was at Furukawa Electric Co., Ltd., where he developed award-winning high-power pump lasers, and patented multi-wavelength-pumped fiber Raman amplifiers. From 1994 to 1997, he was a Visiting Scientist at the Massachusetts Institute of Technology, Cambridge, where he studied mode-locked fiber lasers and ultra-short pulses in fiber. In

2005, he moved to the National Institute of Advanced Industrial Science and Technology (AIST), Tsukuba, Japan, where he has served as Executive Committee Chair of a ten-year national project called “Vertically Integrated Center for Technologies of Optical Routing toward Ideal Energy Savings (VICTORIES)” in collaboration with ten telecom-related companies, and is currently Deputy Research Director of Electronics and Photonics Research Institute in AIST. He has authored or coauthored more than 500 conference presentations, papers, book chapters, articles, and patents. His current research interests include software defined dynamic optical path networking and their enabling devices such as nonlinear fiber-optics and silicon photonics. He was an Associate Editor and Advisory Editor of Optics Express and the Co-Editor-in-Chief of the IEICE Transactions on Communications. He was on the technical committee for OFC, ECOC, CLEO, OECC, OAA, etc. and served as Program Co-Chair of OFC 2015, and General Co-Chair of OFC 2017. Dr. Namiki is a Fellow of OSA and IEEE, and a member of IEICE and JSAP.



Hitoshi Kawashima received his PhD in chemistry in 1993 from Kyoto University, Kyoto, Japan. He was a postdoctoral fellow at MIT from 1993 to 1995, where he worked on pulse-shaping technology for femtosecond optical pulses. In 1995, he joined the Electrotechnical Laboratory. In 2001, the Electrotechnical Laboratory and other fourteen national research laboratories were reorganized and renamed as the National Institute of Advanced Industrial Science and Technology (AIST). Since 2008, he

has worked on silicon photonics and its applications to circuit switches. His research interests include integrated optics, nonlinear optics, and diagnostic techniques with ultrashort optical pulses. He is a member of OSA, IEICE, and Japan Society of Applied Physics.



Kazuhiro Ikeda received his BE and ME degrees in precision science from the Osaka University, Suita, Japan, in 1998 and 2000, respectively, and the PhD in Electrical Engineering (Photonics) from the University of California, San Diego (UCSD), La Jolla, USA, in 2008. His doctoral thesis was on nonlinear optical responses in silicon nitride and amorphous silicon and developed sidewall corrugated waveguide devices, all for silicon photonics applications.

From 2000 to 2004, he worked for the Furukawa Electric Co., Ltd. on polarization controllers and polarization mode dispersion compensators for optical fiber communications. In 2009, he joined the Graduate School of Materials Science, Nara Institute of Science and Technology (NAIST), Ikoma, Japan, as an Assistant Professor, where he studied opto-spintronics and plasmonic microresonators for semiconductor lasers. Since 2014, he is a research group leader with the National Institute of Advanced Industrial Science and Technology (AIST), Tsukuba, Japan. Dr. Ikeda is a senior member of the OSA and a member of the IEICE, JSAP, and IEEE Photonics Society. His research interests include silicon photonic integrated circuits and hybrid nanophotonics on silicon.